

---

# DEFORMIRISNET: AN IDENTITY-PRESERVING MODEL OF IRIS TEXTURE DEFORMATION

---

Siamul Karim Khan, Patrick Tinsley, Adam Czajka

University of Notre Dame

{skhan22, ptinsley, aczajka}@nd.edu

## ABSTRACT

Nonlinear iris texture deformations due to pupil size variations are one of the main factors responsible for within-class variance of genuine comparison scores in iris recognition. In dominant approaches to iris recognition, the size of a ring-shaped iris region is linearly scaled to a canonical rectangle, used further in encoding and matching. However, the biological complexity of iris sphincter and dilator muscles causes the movements of iris features to be nonlinear in a function of pupil size, and not solely organized along radial paths. Alternatively to the existing theoretical models based on biomechanics of iris musculature, in this paper we propose a novel deep autoencoder-based model that can effectively learn complex movements of iris texture features directly from the data. The proposed model takes two inputs, (a) an ISO-compliant near-infrared iris image with initial pupil size, and (b) the binary mask defining the target shape of the iris. The model makes all the necessary nonlinear deformations to the iris texture to match the shape of iris in image (a) with the shape provided by the target mask (b). The identity-preservation component of the loss function helps the model in finding deformations that preserve identity and not only visual realism of generated samples. We also demonstrate two immediate applications of this model: better compensation for iris texture deformations in iris recognition algorithms, compared to linear models, and creation of generative algorithm that can aid human forensic examiners, who may need to compare iris images with large difference in pupil dilation. We offer the source codes and model weights available along with this paper.

## 1 Introduction

The human iris is a thin, circular structure presenting a rich and unique texture information defined by detailed characteristics such as crypts, ridges, furrows, rings, corona, freckles, and a zigzag collarette. The minute iris patterns and textures are formed during gestation and have relatively little influence from genes [8], making it unique even for the identical twins, and different in our left and right eyes. Due to its uniqueness and stability, iris texture is one of the most reliable biometric traits widely employed for recognition. Recent research results [20] also suggest that iris recognition is feasible a few weeks after death, which opened interesting additional applications to forensic identification.

One of the primary sources of within-class variance in this biometric modality is the highly complex iris texture deformation due to pupil size variation. Dominant approaches to iris recognition based on Daugman's method [7] map the iris annulus into a rectangular region of canonical dimensions. While simple and effective, this linear mapping does not compensate for large differences in pupil size [10] and nonlinear mapping, modeling some but not all of the possible iris texture deformation subtleties [19], was found to be a better choice.

In this paper, we propose an **end-to-end deep-learning-based model of complex iris texture deformation**, and demonstrate its usefulness in two applications: iris recognition (to match the pupil size between iris scans being compared) and human forensic iris examination. The model does not assume circularity of iris boundaries, and is able to process ISO-compliant [11] full-frame iris images (not only their normalized versions).

In particular, we propose an autoencoder trained with identity-preserving loss that deforms an input iris image to match its new shape given by an input mask, as shown in Fig. 1. The proposed method is trained to appropriately

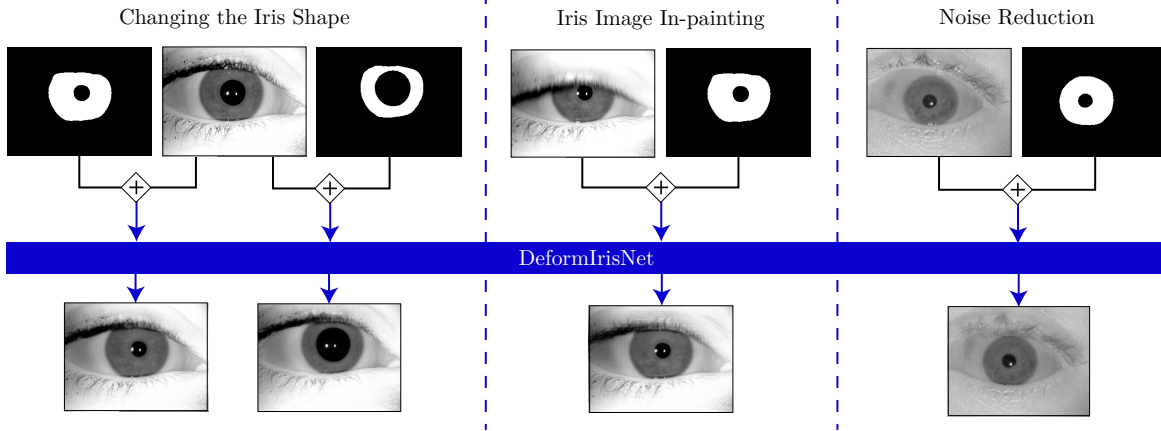


Figure 1: The proposed model (DeformIrisNet) deforms an input iris image (**left**) to match the requested shape of the iris given by the target mask (also provided as an input), preserving the identity and improving the iris recognition compared to linear normalization methods. Deformation is made in a way to mimic the authentic, very complex iris muscle movements. Additionally, the proposed model can “inpaint” iris texture in places covered by eyelids in the input sample (**middle**) and reduce selected types of noise in the input image when we do not request the change in iris size (**right**).

capture the complex, non-linear dynamics of the iris texture and generate iris images with dilated pupil which can allow for better iris recognition performance. Our model can also aid human examiners in better comparing iris image pairs with excessive differences in pupil size, what was found to be one of the biggest confusion source for subjects comparing iris images [16]. We also show that an intuitive approach employing components of modern Generative Adversarial Networks may offer results (in terms of identity preservation) that are inferior to those obtained with the proposed autoencoder-based model. We offer source codes and model weights along with this paper.

## 2 Related Works

The most commonly used method for iris normalization is the homogeneous rubber sheet model proposed by Daugman [8] which maps every pixel  $(x, y)$  of the iris annulus in the Cartesian coordinate system into an equivalent pixel in the polar coordinate system  $(r, \theta)$ , where  $r \in [0, 1]$  is the radial distance from the inner iris boundary, and  $\theta \in [0, 2\pi]$  is the angular position. This model essentially converts the circular iris region into a canonical rectangular image, compensating linearly for pupil size variations. Hollingsworth, Bowyer *et al.* have shown, however, that despite this linear normalization, pupil dilation can degrade iris recognition performance [10, 5].

There are relatively few advances in iris normalization compared to iris segmentation and iris feature extraction. Tomeo-Reyes *et al.* [19] addressed the problem of pupil dilation by proposing the biomechanical model of iris muscle deformation. They model the iris region as a thin cylindrical shell made of orthropic material and utilize the biomechanics of the iris region to calculate the displacements that occur during iris dilation and constriction. This model can compensate for some, but not all nonlinear movements of iris features, as it is a significant simplification of the dynamics of the iris musculature.

Wilde *et al.* [22] compensated the iris deformation using an image registration technique. The technique searches for an optimal transformation in both space and intensity that maps each point from one image to a point in the other. Wei *et al.* [21] proposed an alternative non-linear iris normalization model based on statistical learning. The proposed iris deformation model is a combination of linear and non-linear stretch. The linear stretch is based on the rubbersheet model and the non-linear stretch is modeled using a Gaussian function with parameters obtained by training. Yuan *et al.* developed a non-linear iris normalization method based on the minimum-wear-and-tear meshwork of the iris [24]. The minimum-wear-and-tear meshwork proposed by Wyatt [23] models the iris as a mesh of radial and circular muscles and estimates the deformation based on the motion of this mesh work. Lefevre *et al.* suggests a rubber sheet model based on fitted ellipses instead of circles [14].

More recently, Generative Adversarial Networks-based approaches have also been experimented with to vary pupil size, but most of such methods suffer from “texture sticking” problem and thus cannot preserve the identity properly.

The proposed model **is different from the the previous work** in two ways. First, it makes neither geometrical or biological assumptions about the iris constriction phenomenon, nor requires providing the “pupil size” (which is actually difficult to define due to irregular shape of the pupil). The proposed model learns the complex iris muscle movement directly from the data. Second, the model works directly with ISO-compliant iris scans (*i.e.*  $640 \times 480$  pixel near-infrared images), what makes the model applicable to complement *any* iris matcher, including “black box” or closed commercial matchers.

### 3 Database

We utilize the Warsaw-BioBase-Pupil-Dynamics v3.0 (WBPD) dataset which consists of 30-second-long near-infrared iris videos with variable pupil size due to visible-light stimuli [13]. After 15 seconds, a visible light stimulus caused pupil contraction, which was kept for 5 seconds, and then followed by a restorative dilation. After converting original videos to images, the dataset contains 117,117 grayscale images at a resolution of  $768 \times 576$ . The dataset contains images from 84 different eyes.

A necessary data curation step was to pair small and large pupil images in a way that allows us to provide appropriate inputs and targets to train the proposed model. To do that, we first automatically detect the pupil and iris radii for all the images in the dataset and find the pupil-to-iris ratio. Previous research has shown that pupil-to-iris ratio generally varies between 0.2 (highly constricted pupil) and 0.7 (highly dilated pupil) [10, 19]. We take all the images with pupil-to-iris ratio between 0.2 and 0.7, and divide it into 5 bins of width 0.1; that is, the first bin contains all images with pupil-to-iris ratio between 0.2 and 0.3, second bin contains all images with pupil-to-iris ratio between 0.3 and 0.4, and so on. As we are concerned with training a model for dilation, for images in each bin, we pair it with images from all the bins with a higher pupil-to-iris ratio.

We divide the data into training, validation and test sets based on the different eyes, with 67 of the eyes in the training set, 6 in the validation set, and 7 in the test set. This eye-disjoint split is crucial to make sure the model is learning generic iris muscle movements, and not dynamics specific to subjects present in the dataset.

## 4 Proposed Method

### 4.1 Overview

We propose a modified U-Net autoencoder which is trained to construct a new image with an iris matching the shape (including size) delivered by the image mask provided also as input. Though, it is not the autoencoder architecture that is our contribution, and rather its training mechanism with multiple loss components, that ends up with a possibility to learn complex iris muscle movements to generate images that not only preserve the identity, but even help in iris recognition.

Figure 2 presents an overview of the model’s training strategy. There are several components of the proposed loss function, which can be grouped into two functional components: identity preservation component and perceptual realism preservation component. The next two subsections describe these two aspects of this training in details.

### 4.2 Identity Preservation

To preserve the identity of the iris while training the autoencoder, we define a loss that specifically focuses on identity preservation. First, we convert the iris regions of both the output and the target from Cartesian coordinates to a pseudo-polar coordinate system as defined by Daugman’s rubber sheet model [8]. For an image  $I$  with iris center  $(x_i, y_i)$ , iris radius  $r_i$ , pupil center  $(x_p, y_p)$  and pupil radius  $r_p$ , we can build a normalized iris image as a function  $N_D$  giving an output image  $O$  of width  $w_D$  and height  $h_D$  as:

$$O = N_D(I) \tag{1}$$

where

$$O(r \times h_D, (\theta/2\pi) \times w_D) = I(x(r, \theta), y(r, \theta)) \tag{2}$$

$$x(r, \theta) = (1 - r) \times (x_p + r_p \times \cos(\theta)) + r \times (x_i + r_i \times \cos(\theta)) \tag{3}$$

$$y(r, \theta) = (1 - r) \times (y_p + r_p \times \sin(\theta)) + r \times (y_i + r_i \times \sin(\theta)) \tag{4}$$

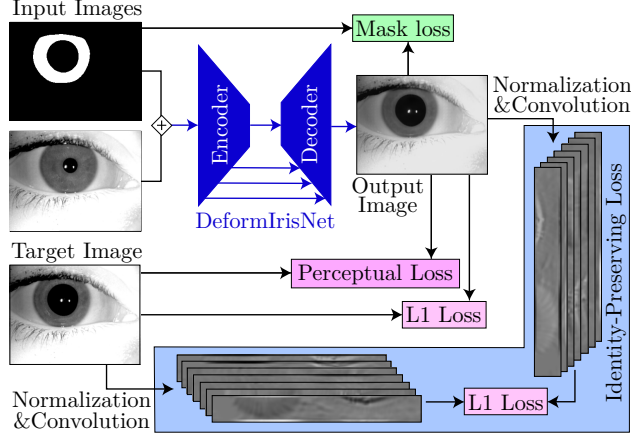


Figure 2: Illustration of the training mechanism with all loss components: (a) “Mask Loss” to request new shape of the iris, (b) “Identity-Preserving Loss” for constraining the deformations to those mimicking the authentic iris muscle movements, hence preserving the identity information in the generated sample, (c) “L1 Loss” to maximize general similarity of the generated and ground-truth images, and (d) “Perceptual Loss” used to maximize perceptual realism of the generated samples.  $\diamond$  denotes concatenation across channels.

with  $r \in [0, 1]$  and  $\theta \in [0, 2\pi]$ . Basically, the rubber sheet model “unrolls” the iris region onto a rectangular region of a specified width and height.

In the next step, we utilize the iris domain-specific ICA filters  $F_{iris}$  [6] that were learned using image patches extracted from human salient regions obtained from an eye tracking device. We decided to use this iris feature extractor due to reported best recognition accuracy across all open-source iris matchers by a couple of teams [4, 9]. In particular, the identity preservation loss component is defined as:

$$L_{identity} = |F_{iris} \otimes N_D(I_O) - F_{iris} \otimes N_D(I_T)| \quad (5)$$

where  $\otimes$  denotes the convolution operation. In words, we convolve the filters with the output iris images  $I_O$  from the autoencoder, and target iris images  $I_T$  after iris texture normalization  $N_D$ , and take the mean absolute error between these results as the identity-preserving loss.

### 4.3 Maintaining Realism

To match the shape of the generated iris with the desired shape (given by the input mask), we use the lightweight CC-Net [15] model, trained for iris segmentation task, to find the logits for both of the images, and then minimize the absolute difference between the logits (“Mask Loss” in Fig. 2). This construction is differentiable and fast, so this enables us to use it in the autoencoder loss function without a significant slowdown in training.

To ensure visual realism in the output images, we use the Learned Perceptual Image Patch Similarity (LPIPS-v0.1) loss (“Perceptual Loss” in Fig. 2) which matches deep features extracted from the AlexNet backbone to ensure the output image is “perceptually” similar to the target image [25]. We also add the L1 norm between the generated sample and ground truth (“L1 Loss” in Fig. 2) which essentially tries to match the output and target image directly. Ideally, if we had infinite data and complex enough model architecture, this “L1 loss” would have been sufficient to effectively train our model. Practically however, we need to build a mechanism into the overall training strategy that guides the network towards salient iris features in case when data is limited.

### 4.4 Choosing a Neural Network Architecture

Since it is currently one of the most popular off-the-shelf generative adversarial networks (GANs), we initially experimented with the StyleGAN3 [12] generator as a decoder to generate the output iris images. The generator model was trained from scratch on a subset of the WBPD dataset at a resolution of  $512 \times 512$ . Before initiating the generator training process, data pre-processing included center-cropping the raw images to a square shape ( $512 \times 512$ ) as well as removing raw images wherein the iris was located too close to the image boundary. Additionally, we filtered the training data to exclude iris images where little to no iris was present, such as when a subject was blinking. Left-right mirror augmentation was enabled during training, which effectively doubled the training data

size. After training the generator and getting visually pleasing iris images, we took the generator, froze its weights, and trained an encoder to find the appropriate latent space representations that can preserve the identity. To train this encoder, we followed the training procedure as shown in Figure 2 without the perceptual loss component as this loss aims to create visually pleasing results and our belief was that as the generator can already produce visually appealing results, this loss would be redundant. One thing to note is that the autoencoder architecture that resulted from this did not contain skip connections as shown in Figure 2.

Surprisingly, this intuitive approach ended up with disappointing results, which we thought would be still interesting to share as a “negative” yet useful information. Namely, we found that learning to find the latent space representation using an encoder in this way can neither preserve the identity nor produce visually appealing iris images.

#### 4.5 Architecture Details

We utilize an autoencoder architecture with skip connections belonging to the family of U-Net architectures. Most U-Net architectures are optimized for image segmentation. Thus, to make U-Net “better” at generating iris images, not only segmentation results, we propose changes in the downsampling and upsampling operations detailed below.

For downsampling, we replace maxpooling in the original U-Net autoencoder with a combination of strided convolution and bilinear downsampling followed by convolution in parallel. In max pooling, gradients flows through only the max point and it works great when we want to detect if a feature appears or not and when features are sparse. For our problem, we are looking to capture overall features (the overall iris texture and its dynamics) and the information is not sparse. Our idea is that through strided convolution, the model can learn the most important features it wants to preserve while the downsampling through interpolation would provide the model with a view of the overall features as well.

For upsampling, we add bilinear upsampling followed by convolution in parallel to upsampling by sub-pixel convolution [18, 3]. Using transposed convolution, as in the original U-Net, has been known [17] to cause checkerboard artifacts in the produced image, especially when the kernel size is not divisible by the stride causing uneven overlap of the kernel while sliding over the image. While the transposed convolution used in the original U-Net architecture had a kernel size and stride of 2, we found that replacing it as detailed decreases artifacts in the produced image and thus improves the performance of the iris recognition applied to images generated by this model. Figure 3 shows the overall architecture of our network.

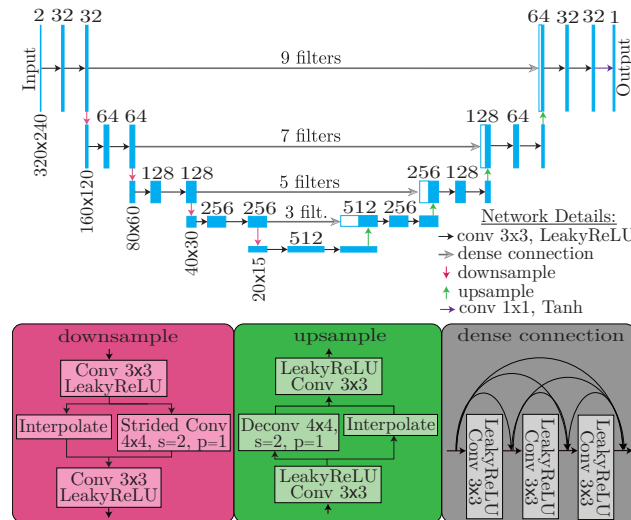


Figure 3: Details of the proposed model and its modules. The bottom figure shows detailed implementation of connections pictured in the top figure. The dense connections (illustrated in the bottom right picture) are explained for three filters; same logic follows for other number of filters.

## 5 Applications

There are two biometric applications of the proposed model. First, a model capable to generate ISO-compliant iris images with varying pupil size, and deforming the iris texture as the authentic eye does, should increase the accuracy of any iris matcher by comparing images with rectified pupil size, instead of raw iris scans. Second, visually-realistic and identity-preserving iris images of varying pupil size can increase the accuracy of human examination in forensics. We present details of these two applications in the following subsections.

### 5.1 Iris Recognition

The usefulness of the the proposed model in iris recognition is evaluated on the subject-disjoint test set of Warsaw-BioBase-Pupil-Dynamics v3.0 [13] (WBPD). The example iris recognition method utilized here is based on human-driven binary image features [6]. We compare our method with the linear model by Daugman [8] (denoted later as “Linear”) and the nonlinear biomechanical model by Tomeo-Reyes et al. [19] (denoted later as “Biomech”).

As there can be a huge number of pairs if we make all possible comparisons for the WBPD dataset, we randomly select image pairs from minimum pupil-to-iris ratio (0.1 to 0.2) bin and maximum pupil-to-iris ratio (0.7 to 0.8) bin without replacement for each individual. We find the genuine and imposter comparisons using these pairs. As we are selecting the pairs randomly, we repeat the experiment 10 times to assess statistical significance of the results.

Table 1: Average percentage of different iris code bits for genuine and imposter comparisons and for various iris texture deformation models.

Method	Genuine pairs	Impostor pairs
Linear [8]	32.67 ± 0.22	43.81 ± 0.15
Biomech [19]	32.74 ± 0.21	43.78 ± 0.16
DeformIrisNet (proposed)	22.40 ± 0.11	34.02 ± 0.08

The iris recognition method used in this evaluation provides unique binary codes for iris textures of different individuals. Table 1 reports the percentage of bits that are different for the binary codes between authentic gallery images (with smaller pupil) and rectified probe images (with the pupil size matching the size of the authentic gallery samples) for all transformation methods. As we can see from the table, the dilated pupil image generated by DeformIrisNet has lower number of disagreeing bits between authentic gallery and rectified genuine probe image than in case of other methods. This is good and expected as deformed iris images are now closer to authentic images. However, we also observe lower number of disagreeing bits for imposter comparisons, what is not desired. Thus, to evaluate the efficacy of the DeformIrisNet model in terms of biometric identification capabilities when used in conjunction with an iris recognition module, we find the genuine and imposter scores distribution for all the iris normalization methods and calculate the sensitivity index ( $d'$ ) defined as:

$$d' = \frac{|\mu_1 - \mu_2|}{\sqrt{\frac{1}{2}(\sigma_1^2 + \sigma_2^2)}} \quad (6)$$

We also calculate the Equal Error Rate (EER) for all the methods.

Table 2: Decidability score  $d'$  and Equal Error Rates (EER) obtained in **same-dataset subject-disjoint evaluation**.

Method	$d'$	EER
Linear [8]	2.642 ± 0.072	0.121
Biomech [19]	2.644 ± 0.062	0.115
DeformIrisNet (proposed)	3.003 ± 0.049	0.118

As shown in Table 2, we find that using the DeformIrisNet model a higher separation between imposter and genuine score distributions (larger  $d'$ ) can be achieved, indicating that the our model is able to produce rectified iris images that are closer to the actual images than those obtained by linear or biomechanical-based normalization strategies. While EER is on par with other method, the receiver operating characteristic (ROC) curves shown in Figure 4 suggest that the example iris recognition method when applied to images rectified with the proposed nonlinear iris deformation model, obtains a better recognition accuracy, measured by Area Under the Curve.

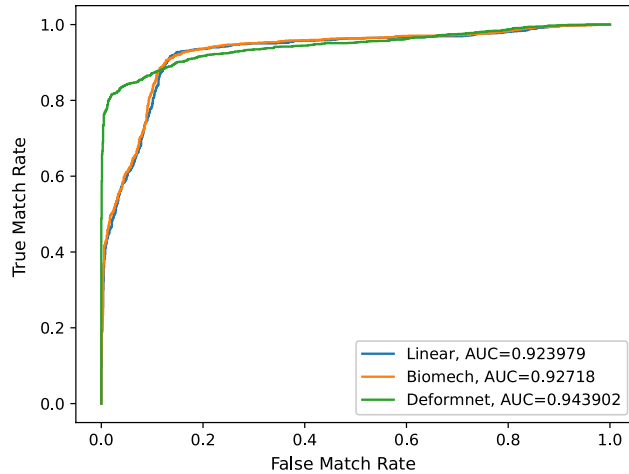


Figure 4: ROC curve and Area Under the Curve values for iris recognition with different iris texture deformation methods: Linear [8], Biomech [19], and DeformIrisNet (proposed)

## 5.2 Human Examination

With iris recognition becoming the next biometric modality in e-passports, a component of the FBI’s Next Generation Identification (NGI) system [1], and recently documented its usefulness for identification of deceased subjects [20], the need for having trained (professional) human iris examiners, who could confirm the machine’s decision in a legally-binding manner started to emerged. For instance, NIST has initiated a working group that meets regularly and aims at designing training curriculum for human iris image examiners who might be called upon to give testimony in court [2].

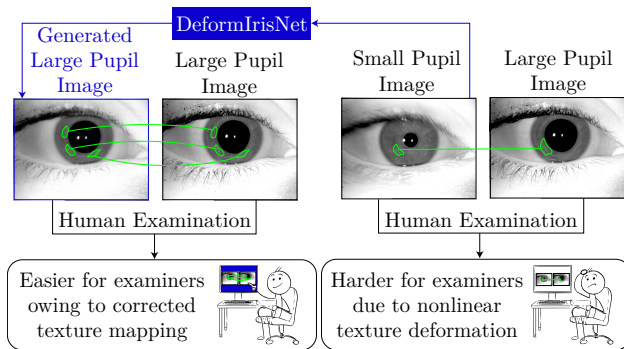


Figure 5: Comparing iris images with the same pupil size is much easier for human examiners than samples with excessive difference in pupil size. DeformIrisNet can be used to rectify the size of the iris annulus, applying correct, learned from the data nonlinear warping of iris texture.

The proposed deformation model may become a useful part of the human examination toolbox. As demonstrated in the literature [16] and illustrated in Figure 5, human examiners may have a tough time comparing iris images from the same individual with excessive difference in pupil size in both samples. Our iris deformation model allows to generate iris images with varying pupil sizes from a still iris image. That is, the human examiner, by rotating a virtual “knob”, can generate infinite number of samples preserving the identity and showing the iris at various levels of constriction to match the desired pupil size. The supplementary materials include a video showing an example output of such process, and in Fig. 6. Such a tool should significantly increase the chances to correctly match iris samples under examination, and to our knowledge has never been proposed before.

Figure 7 additional shows the result of running multiple iris images with different pupil sizes through DeformIrisNet and requesting the same pupil size for all samples. An interesting observation here is that the smaller the change in pupil is, the sharper and closer the output image is to the input image. This should be the case because the smaller the difference in the pupil size, the “lesser” the work that our model needs to do to deform the iris image and match the input pupil mask.

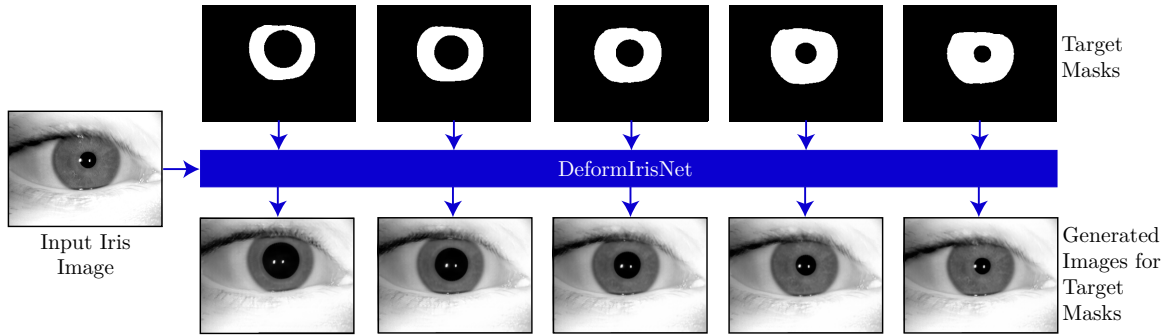


Figure 6: Iris images generated by DeformIrisNet from a single iris sample (left), given the target masks (top) that can be used in human examination of iris image pairs, making the process easier for forensic examiners when examined iris scans with varying pupil size.

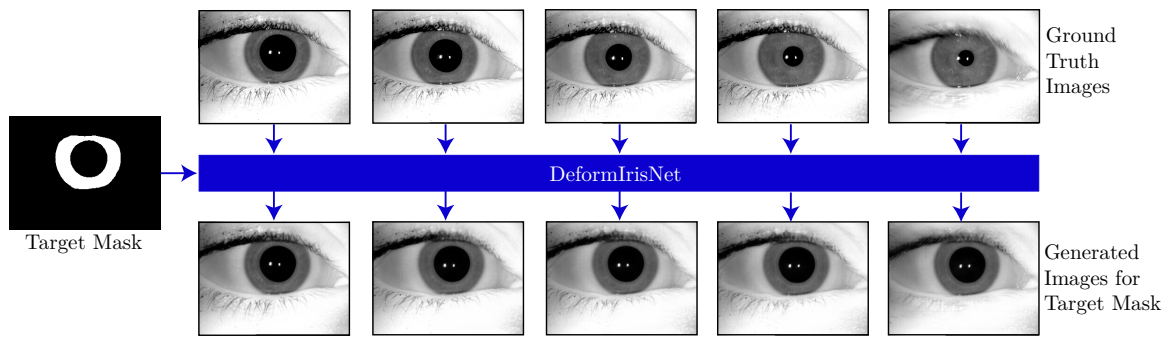


Figure 7: Same as in Fig. 6, except that illustrating generative process from multiple images of varying pupil size into a single iris images with a canonical pupil size.

## 6 Iris Inpainting and Noise Reduction

Apart from two core applications driven by actual and timely needs in iris recognition community, the proposed model can be also used for “painting” realistically-looking iris NIR images given arbitrary iris mask. Also, it can be applied as a noise reduction tool. This subsection discusses these two additional applications.

In the training dataset we utilized, there are iris images with partially closed eyelids when subject was blinking. Interestingly, seeing such examples during training, the model learned how to “open” or “close” the eyelids given the mask suggesting such situations. Figure 8 shows what happens when we take an iris image and run it through the model together with masks for partially closed eye images. We see that the network effectively learned to close the eyelid while preserving the iris texture for the visible region.

Figure 9 shows what happens when we take iris image with partially closed eyelids and run it through the model with a target mask suggesting a fully opened eye. Interestingly, if a significant portion of the iris texture is visible, the rest of the iris texture is being “dreamed” up by the network in a way to make it similar to the actual iris texture, but – certainly – without a guarantee that the generated texture represents a given identity.

Finally, Fig. 10 demonstrates how the trained DeformIrisNet can partially de-noise iris images by feeding it with a noisy iris image and actual segmentation mask for that image (so no changes in iris texture are requested). While it is not perceived as a main application of the trained model, we found it an interesting by-product for the model that “understands” the complex deformations of the iris texture.

## 7 Conclusion

This paper proposes an end-to-end, fully data-driven autoencoder-based approach to mimic complex deformations of the iris texture while preserving the identity information of an individual whose iris image is being processed. We demonstrated its potential usefulness in two applications: (a) iris recognition and (b) forensic human examination. Since the rectified iris images are compliant with ISO requirements, they can be used with any iris



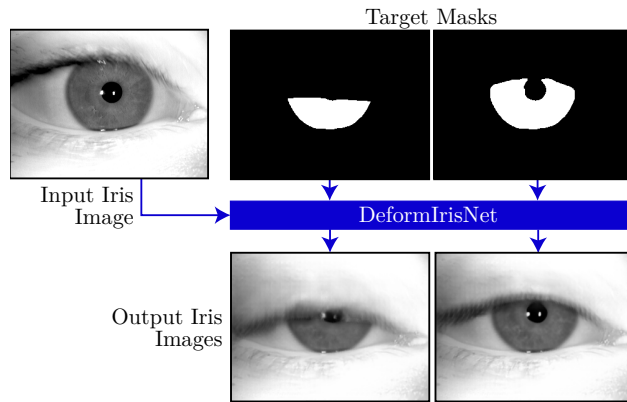


Figure 8: Generating partially closed eye images from an open eye image given the segmentation mask.

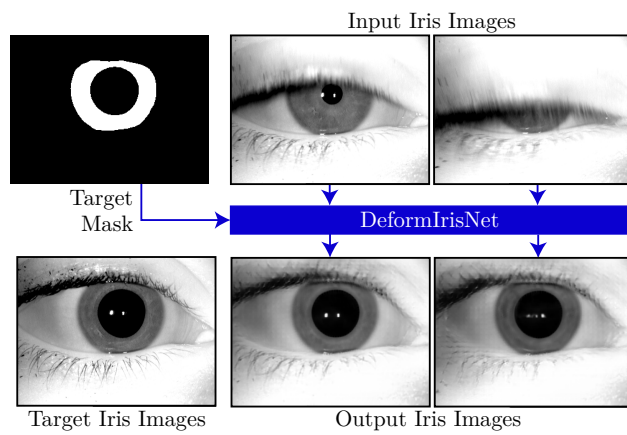


Figure 9: Generating an open eye image from partially closed eye image given the segmentation mask.

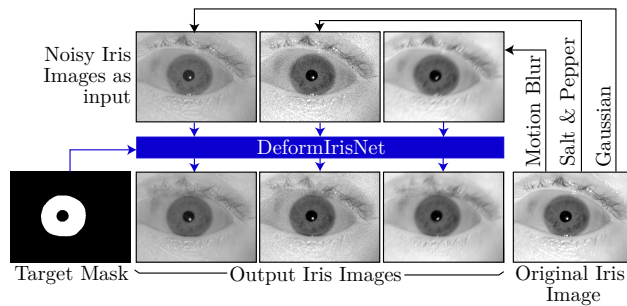


Figure 10: An example of what happens when we run a noisy version of the image through the network.

recognition methods, including black-box / closed-source commercial solutions. Matching the iris images with identical pupil size should make it easier for human examiners to compare and match iris scans. In addition, we presented in-painting and noise reduction capabilities of the proposed model. Source codes and model weights are offered along with the paper for full reproducibility and to facilitate further research in this area.

## References

- [1] Next Generation Identification (NGI). <https://www.fbi.gov/services/cjis/fingerprints-and-other-biometrics/ngi>. Accessed: July 11, 2022.
- [2] NIST IEG: Iris Examiner Training Discussion. <https://www.nist.gov/itl/iad/image-group/ieg-iris-examiner-training-discussion>. Accessed: July 11, 2022.
- [3] Andrew Aitken, Christian Ledig, Lucas Theis, Jose Caballero, Zehan Wang, and Wenzhe Shi. Checkerboard artifact free sub-pixel convolution: A note on sub-pixel convolution, resize convolution and convolution resize. *arXiv preprint arXiv:1707.02937*, 2017.
- [4] Mauro Barni, Ruggero Donida Labati, Angelo Genovese, Vincenzo Piuri, and Fabio Scotti. Iris deidentification with high visual realism for privacy protection on websites and social networks. *IEEE Access*, 9:131995–132010, 2021.
- [5] Kevin W Bowyer, Sarah E Baker, Amanda Hentz, Karen Hollingsworth, Tanya Peters, and Patrick J Flynn. Factors that degrade the match distribution in iris biometrics. *Identity in the information Society*, 2(3):327–343, 2009.
- [6] Adam Czajka, Daniel Moreira, Kevin Bowyer, and Patrick Flynn. Domain-specific human-inspired binarized statistical image features for iris recognition. In *2019 IEEE Winter Conference on Applications of Computer Vision (WACV)*, pages 959–967. IEEE, 2019.
- [7] John Daugman. How iris recognition works. In *The essential guide to image processing*, pages 715–739. Elsevier, 2009.
- [8] John G Daugman. High confidence visual recognition of persons by a test of statistical independence. *IEEE transactions on pattern analysis and machine intelligence*, 15(11):1148–1161, 1993.
- [9] R. Donida Labati, Angelo Genovese, Vincenzo Piuri, Fabio Scotti, and Sarvesh Vishwakarma. I-social-db: A labeled database of images collected from websites and social media for iris recognition. *Image and Vision Computing*, 105:104058, 2021.
- [10] Karen Hollingsworth, Kevin W Bowyer, and Patrick J Flynn. Pupil dilation degrades iris biometric performance. *Computer vision and image understanding*, 113(1):150–157, 2009.
- [11] ISO/IEC 19794-6:2011. Information technology – Biometric data interchange formats – Part 6: Iris image data, 2011.
- [12] Tero Karras, Miika Aittala, Samuli Laine, Erik Härkönen, Janne Hellsten, Jaakko Lehtinen, and Timo Aila. Alias-free generative adversarial networks. In *Proc. NeurIPS*, 2021.
- [13] Jeffery Kinnison, Mateusz Trokielewicz, Camila Carballo, Adam Czajka, and Walter Scheirer. Learning-free iris segmentation revisited: A first step toward fast volumetric operation over video samples. In *2019 International Conference on Biometrics (ICB)*, pages 1–8. IEEE, 2019.
- [14] Thierry Lefevre, Bernadette Dorizzi, Sonia Garcia-Salicetti, Nadege Lemperiere, and Stephane Belardi. Effective elliptic fitting for iris normalization. *Computer Vision and Image Understanding*, 117(6):732–745, 2013.
- [15] Suraj Mishra, Peixian Liang, Adam Czajka, Danny Z Chen, and X Sharon Hu. Cc-net: Image complexity guided network compression for biomedical image segmentation. In *2019 IEEE 16th International Symposium on Biomedical Imaging (ISBI 2019)*, pages 57–60. IEEE, 2019.
- [16] Daniel Moreira, Mateusz Trokielewicz, Adam Czajka, Kevin Bowyer, and Patrick Flynn. Performance of humans in iris recognition: The impact of iris condition and annotation-driven verification. In *2019 IEEE Winter Conference on Applications of Computer Vision (WACV)*, pages 941–949, 2019.
- [17] Augustus Odena, Vincent Dumoulin, and Chris Olah. Deconvolution and checkerboard artifacts. *Distill*, 2016.
- [18] Wenzhe Shi, Jose Caballero, Ferenc Huszár, Johannes Totz, Andrew P Aitken, Rob Bishop, Daniel Rueckert, and Zehan Wang. Real-time single image and video super-resolution using an efficient sub-pixel convolutional neural network. In *Proceedings of the IEEE conference on computer vision and pattern recognition*, pages 1874–1883, 2016.
- [19] Inmaculada Tomeo-Reyes, Arun Ross, Antwan D Clark, and Vinod Chandran. A biomechanical approach to iris normalization. In *2015 International Conference on Biometrics (ICB)*, pages 9–16. IEEE, 2015.
- [20] Mateusz Trokielewicz, Adam Czajka, and Piotr Maciejewicz. Iris recognition after death. *IEEE Transactions on Information Forensics and Security*, 14(6):1501–1514, 2019.
- [21] Zhuoshi Wei, Tieniu Tan, and Zhenan Sun. Nonlinear iris deformation correction based on gaussian model. In *International Conference on Biometrics*, pages 780–789. Springer, 2007.
- [22] Richard P Wildes. Iris recognition: an emerging biometric technology. *Proceedings of the IEEE*, 85(9):1348–1363, 1997.
- [23] Harry J Wyatt. A ‘minimum-wear-and-tear’ meshwork for the iris. *Vision Research*, 40(16):2167–2176, 2000.
- [24] Xiaoyan Yuan and Pengfei Shi. A non-linear normalization model for iris recognition. In *International Workshop on Biometric Person Authentication*, pages 135–141. Springer, 2005.
- [25] Richard Zhang, Phillip Isola, Alexei A Efros, Eli Shechtman, and Oliver Wang. The unreasonable effectiveness of deep features as a perceptual metric. In *CVPR*, 2018.